Carbohydrate Polymers 88 (2012) 61–67

Contents lists available at SciVerse ScienceDirect

Carbohydrate Polymers

journal homepage: www.elsevier.com/locate/carbpol

Facile synthesis of three-dimensional chitosan–graphene mesostructures for reactive black 5 removal

Jin-Sheng Cheng[a,b,*], Jin Du[b], Wenjuan Zhu[c]

[a] School of Pharmacy, Zhejiang Chinese Medical University, Hangzhou 310053, China
[b] School of Pharmacy, Guilin Medical University, Guilin 541004, China
[c] Anhui Medical University, Hefei 230026, China

ARTICLE INFO

Article history:
Received 20 October 2011
Received in revised form 8 November 2011
Accepted 18 November 2011
Available online 27 November 2011

Keywords:
Synthesis
Three-dimensional
Graphene
Mesostructures
Reactive black 5

ABSTRACT

In this paper, a hydrophilic and biocompatible three-dimensional (3D) chitosan–graphene mesostructures with large specific surface area (603.2 $m^2 g^{-1}$) and unique mesoporosity were prepared by simply thermal treatment of graphene oxide nanosheets and chitosan. By starting from waste sugarcane bagasse derived graphite and chitosan, the resulted 3D nanocomposites possess superior competitiveness in biocompatibility, renewable resource recycling, cheapness and specific area. The composites were systematically characterized by a variety of analytical methods. Investigations showed that the 3D mesostructures can be used to remove reactive black 5 (RB5) from aqueous solution. A removal efficiency of 97.5% can be achieved readily at initial RB5 concentrations of 1.0 mg/mL. These results indicate the 3D mesostructures can be used to treat the industrial effluent or contaminated natural water, providing novel insights for the fabrication of 3D functionalized graphene with various building blocks for broad potential applications.

1. Introduction

Graphene, a one-atom-thick planar carbon material with superior chemical stability, large surface-to-volume ratio, tunable band gap, good electronic, mechanical and thermal stability, is currently attracting considerable attentions (Bunch et al., 2007; Geim, 2009; Li, Wang, Zhang, Lee, & Dai, 2008; Stoller, Park, Zhu, An, & Ruoff, 2008). Various methodologies have been developed to fabricate graphene, which include Scotch tape (Novoselov et al., 2005), epitaxial growth (Reina et al., 2008) and chemical reduction of graphene oxide etc. (Xu, Bai, Lu, Li, & Shi, 2008). All these approaches are suitable to prepare traditional graphene nanosheets, while in some important areas such as energy-storage materials, liquid crystal devices, field effect transistors, biosensors, catalysts as well as adsorbents for water treatment (Allen, Tung, & Kaner, 2008; Li et al., 2008; Wu, Pisula, & Müllen, 2008), graphene based materials with unique pore structures and significantly enhanced specific surface area are urgently needed to achieve high electrical or catalytic performances. Due to gradual decrease of its hydrophilic character, conventional graphene nanosheets are easily aggregated and even restacked to form graphite when they are used with bulk-quantity (Du et al., 2008; Wang, Zhi, & Müllen, 2008), the pristine properties of graphene would be therefore hindered.

Fortunately, previous works show that graphene materials with spatial mesostructures would avoid such inferior possibility of graphene (Fan et al., 2010; Lee et al., 2010). In recently years, three-dimensional mesoporous carbon materials have been fabricated *via* hard templates methods or soft templates methods (e.g. self-assembly) (Chen et al., 2011; Fan et al., 2010; Guo, Hu, Lou, & Li, 2010; Guo, Lu, Lei, & Li, 2010; Lee et al., 2010; Liang, Li, & Dai, 2008; Sun, Guo, Zhu, & Li, 2009; Xu, Sheng, Li, & Shi, 2010; Xu, Wu, Sun, Bai, & Shi, 2010). However, these templating routes suffer disadvantages related to high costs and tedious synthetic procedures. Moreover, such conventional approaches to the production of 3D structures are usually tended to use non-biocompatible graphene materials. Therefore, its necessary to develop a template-free approach for biocompatible 3D mesoporous graphene-based material for broad-scientific research and practical applications. Previous work shows that graphene functionalized with different polymers or ionic liquid would be beneficial for constructing biocompatible 3D mesoporous carbon material (Allen et al., 2008; Guo, Hu et al., 2010; Guo, Lu et al., 2010; Xu, Sheng et al., 2010). Chitosan (CS), the second most abundant natural biopolymer on earth (Kawahara et al., 2003; Macquarrie & Hardy, 2005), possesses excellent film-forming ability, biocompability, biodegradable, good adhesion, non-toxicity, and susceptibility to chemical modification due to the presence of plentiful amino groups and hydroxyl groups.

* Corresponding author. Tel.: +86 773 2295100; fax: +86 773 2295100.
E-mail addresses: chengjs@mail.ustc.edu.cn, chengjins@gmail.com (J.-S. Cheng).

0144-8617/$ – see front matter © 2011 Elsevier Ltd. All rights reserved.
doi:10.1016/j.carbpol.2011.11.065

Based on these specific properties of CS, it is reasonable to speculate that both the hydrophilicity and biocompatibility of graphene could be improved by non-covalent functionalization of graphene with CS, the pristine properties of graphene and CS would be therefore preserved.

Wastewater from industries is highly colored and the residual azo dyes in it are seriously concerned for their adverse effects to human beings and the environment (Crini, 2006; Forgacs, Cserháti, & Oros, 2004). Many technologies have been developed for the azo dyes removal from aquatic environment, including physical, chemical and biological approaches (Ahmad & Puasa, 2007; Stolz, 2001). However, most chemical and biological methods with high cost or low degradation efficiency are rarely used in the actual treatment processes (Crini, 2006; Ghoreishi & Haghighi, 2003), some physical adsorption approaches also encountered low removing efficiencies of dye (Crini, 2006; Forgacs et al., 2004).

In the past several years, graphene and graphene-based functional materials have caused increasing interests in environmental applications due to its large surface area, excellent mechanical strength and high electrical conductivity (Chandra et al., 2010; Yang et al., 2010). For example, we have prepared a chemically bonded TiO_2 (P25)-graphene nanocomposites photocatalyst, which possessed great adsorptivity of dyes, extended light absorption range, and efficient charge separation properties simultaneously and demonstrated significant advancement over bare P25 in the photodegradation of methylene blue dye under both UV and visible light irradiation (Zhang, Lv, Li, Wang, & Li, 2010).

Developing hydrophilic and biocompatible 3D structures graphene composites with large specific surface area and unique mesoporosity by simply thermal method would expand its significance in the area of environmental applications. Herein, a template-free approach is used to controllably synthesize the novel 3D-CSGR mesostructures with large specific surface area and pronounced mesoporosity by simply thermal treatment of the mixture of graphene nanosheets and chitosan. The physcicochemical properties of the 3D material are systematically characterized by Fourier transform infrared (FTIR) spectrometry, transmission electron microscopy (TEM), scanning electron microscopy (SEM), Raman spectroscopy, atomic force microscopy (AFM), X-ray diffraction (XRD) spectroscopy, selected area electron diffraction (SAED) patterns and Brunauer–Emmett–Teller (BET) analysis. The 3D mesostructures were used as an effective absorbent for the decoloration of reactive black 5 (RB5, Scheme 1) with superior performance (Barron-Zambrano, Szygula, Ruiz, Sastre, & Guibal, 2010), which is competitive to commercial absorbents. Moreover, this hydrophilic and biocompatible 3D structures graphene composites with large specific surface area (603.2 $m^2\,g^{-1}$) and unique mesoporosity show also broad prospects in catalyst, solar cell, lithium ions battery and biosensors.

2. Materials and methods

2.1. Materials

Graphite powder (99.99995%, 325 mesh) was purchased from Alfa Aesar. Chitosan was supplied by National Medicine Group, Shanghai, China (the degree of deacetylation was 90%, and the molecular weight was 125,000 g mol^{-1}). The chitosan was ground and sieved, and the 0–125 μm fraction was used for experiments. Sugarcane bagasse (SB) was obtained from Liangci Manufacturing Co. Ltd. of the Guangxi Zhuang Autonomous Region of China. Sugarcane bagasse was activated by physical activation, which involved below steps (Ruiz & Rolz, 1971; Girgis, Khalil, & Tawfik, 1994): (1) carbonization process of sugarcane bagasse by using of a dehydrating agent, sulfuric acid, followed by (2) gasification with carbon dioxide at 900 °C and (3) the carbonization step, concentrated H_2SO_4 was added to bagasse in an optimum ratio of 3:4 (weight ratio). The blend was packed into a Pyrex reactor and heated to 160 °C for 2 h with air. Air was metered into the reactor at the rate of 120 dm^3/s. The resulting carbon was cooled and washed with water until acid free and then dried at 110 °C. Graphene oxide (GO) was prepared by modified Hummers method starting from above bagasse derived graphite (Allen et al., 2008; Cheng, Tang, & Li, 2011; Wu et al., 2008; Xu et al., 2008). Graphene was prepared according previous reports (Xu et al., 2008). All solvents and other reagents were purchased from Beijing Chemicals Co. Ltd. as analytical-grade products.

2.2. Methods

XRD measurements of the samples were recorded on a Bruker D8-Advance X-ray powder diffractometer using Cu Kα radiation (λ = 1.5406 Å) with scattering angles (2θ) of 10–70°. JEOL JEM 1200EX and JEOL JEM 2010 transition electronic microscopy were used for transmission electron microscopy (TEM) analysis and high-resolution transmission electron microscopy (HRTEM, equipped with selected area electron diffraction (SAED) analysis). Samples were prepared by placing one drop of an ethanol suspension of the 3D-CSGR composites onto a copper grid (3 mm, 200 mesh) coated with carbon film. A JSM-7401 scanning electron microscopy (SEM) operated at 20 kV was used to analyze the sample. Atomic force microscopic (AFM) images were taken out using a Nanoscope III MultiMode SPM (Digital Instruments) with an AS-12 ("E") scanner operated in tapping mode in conjunction with a V shaped tapping tip (Applied Nanostructures SPM model: ACTA). The images were taken at a scan rate of 2 Hz. Fourier transform infrared (FTIR) spectra were carried out on a spectrum one (Perkin Elmer) spectrometer from KBr pellets. The N_2 adsorption–desorption analysis was measured on a micromeritics ASAP 2010 instrument.

2.3. Synthesis of 3D chitosan–graphene mesostructures

In a typical synthesis, GO dispersion (1.0 mg/mL in water, 100 mL) was ultrasonicated for 1 h, successively, chitosan solution (80 mg, 5% HAc, 20 mL) was added to the dispersion. The mixture was stirred for 10 h, filtered and dried under vacuum. The obtained solid was marked CSGO and was put into an alumina boat, and heated at 150 °C for 45 min under argon flow. After vacuum dried, the 3D chitosan–graphene mesostructures were finally afforded (marked 3D-CSGR). For comparison, CSGR was also prepared by simply reduction of CSGO with hydrazine hydrate at 80 °C for 24 h.

2.4. Absorption of RB5 by 3D-CSGR mesostructures

3D-CSGR (2.0 mL, 0.25 mg/mL, pH 6) was mixed with 4 mL of RB5 (pH 6, 0.2–2 mg/mL) in an erlenmeyer flask. The suspension was incubated at 25 °C for 40 min and standing for another 40 min. Except mentioned specifically, the following absorption experiments were performed according the same protocol. The equilibrium concentration (C_e) was calculated referring to the standard cure of RB5 (the standard curve was drawn based on Lambert–Beer Law: $A = kbc$). The equilibrium sorption capacity (q_e) was calculated by $(C_0 - C_e)/C_{3D\text{-}CSGR}$, where C_0 is the initial concentration of RB5 and $C_{3D\text{-}CSGR}$ is the concentration of 3D-CSGR. The removal efficiency was calculated by $(1 - C_e/C_0) \times 100\%$. The absorption was fitted to both Langmuir model and Freundlich model (Masel, 1996). Batch experiments were conducted to compare the efficiencies of 3D-CSGR to decolorize RB5 in aqueous solution. Dye solutions were prepared in deionized water at initial concentration of 0.25–2 mg/mL of RB5. The 4 mL of dye solution was moved to 10 mL Erlenmeyer flask and then 2 mL 0.25 mg/mL dispersion of 3D-CSGR was added. The flask was incubated at 25 °C

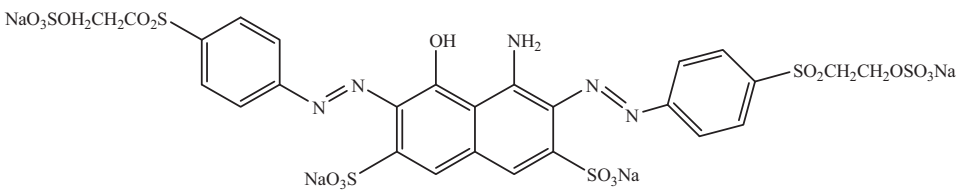

Scheme 1. Structure illustration of reactive black 5 (RB5), a typical azo dye widely used for dying cotton, wood and silk.

for 40 min and stood for another 40 min. The experiment was performed in triplicate and conducted at room temperature. Samples were collected in at 0, 10, 20, 30, 40, 50, 60, 70 and 80 min, respectively. The residual concentrations of RB5 were quantified by UV-3900 spectrophotometer at 598 nm for RB5. To investigate the effect of initial pH on decolorization of RB5 by 3D-CSGR, the dye solution was adjusted pH at 4, 6, and 8 using 0.5 M HCl and 0.5 M NaOH before treatment by 3D-CSGR.

The influence of temperature (0, 25, 50 °C) on the absorption was investigated by incubating the mixture at different temperatures. RB5 adding 2D-CSGR and RB5 without adding any absorbent were treated by the same way for comparison.

3. Results and discussion

3.1. Synthesis and characterization of 3D chitosan–graphene mesostructures

Chitosan is widely used in environmental applications for dye removal owing to its easy degradation, biocompability, biodegradable, low price and large surface area (Barron-Zambrano et al., 2010; Kawahara et al., 2003; Macquarrie & Hardy, 2005). Successful surface modification of grapheme with chitosan by nonfunctional method can combine advantageous properties of graphene and chitosan in environmental applications without loss of their inherit characteristics. To expend its price competitiveness, in this work, graphene was prepared starting from sugarcane bagasse derived graphite instead of commercial one. 3D-CSGR mesostructures would hold much larger specific surface area and unique mesoporosity, further expanding its significance in the area of dye removal, catalyst, or biosensor.

By non-covalent functionalization with chitosan and subsequent thermal treatment of the mixture of GO and chitosan, the 3D-CSGR mesostructures were afforded readily, through this kind of approach, the pristine properties of graphene would be therefore preserved. By starting from cheap sugarcane bagasse derived graphite and chitosan, the resulted composites possess good competitiveness. The XRD patterns of 3D-CSGR in Fig. 1 indicate that 3D-CSGR mesostructures have a peak at $2\theta = 24.7^\circ$, the characteristic peak of graphene (Cheng, Du, & Xu, 2011), confirming the structure of the graphene based 3D-CSGR.

Fig. 2 shows the FTIR spectra of graphene and 3D-CSGR. Compared with the pristine graphene, curve b in Fig. 2 shows two bands of the glucopyranose rings, appearing at approximately 890 and 1150 cm^{-1}, respectively, indicating the existence of the chitosan. The characteristic peak of graphene is 1545 cm^{-1} (attributed to skeletal vibrations of graphene), which could be observed on both curves a–b in Fig. 2, implying the successfully combination of the chitosan to graphene in 3D-CSGR mesostructures.

The structures of 3D-CSGR are further characterized by using SEM. As shown in Fig. 3a, the 3D-CSGR sample possesses mesoporous structures resulted from thermal exfoliation. The mesopores with variable sizes are randomly distributed on the 3D-CSGR composites with highly fluctuant structures. Such pores with different sizes (in the size range of 100–800 nm) are generated due to that the oxygen-containing groups of GO and chitosan would

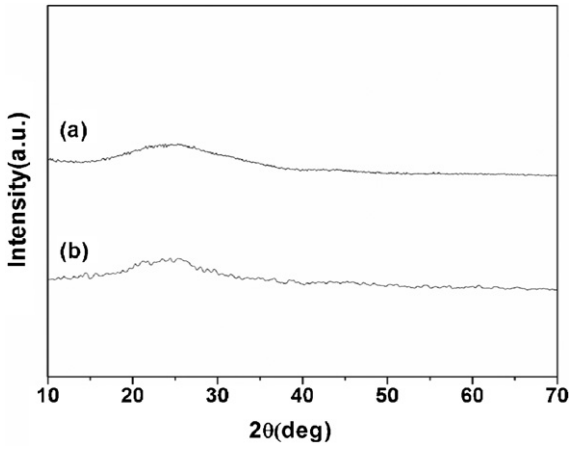

Fig. 1. XRD patterns of graphene (a) and the 3D-CSGR mesostructures (b).

decompose into CO_2 and H_2O by thermal treatment. The chitosan component in this composites changes to an extended two-fold helix (the annealed polymorph) stabilized by an intramolecular O(3)–O(5) by removal of the residual acid and thermal treatment (Kawahara et al., 2003), leading to the formation of unique mesoporosity and three-dimentional structures (Guo, Hu et al., 2010; Guo, Lu et al., 2010). Further magnified SEM image shown in Fig. 3b reveals that the 3D-CSGR composites have delaminated structures, in these layers of such delaminated 3D composites, one could even observe easily the paper-like wrinkled structures of graphene, indicates that the 3D-CSGR product is made up of graphene nanosheets. Moreover, Fig. 3b demonstrates that the typical pore sizes are about 100 and 500 nm. TEM image in Fig. 3c illustrates the thinnest section of 3D-CSGR composites, confirming that the sample has 3D structures. In the image of lower left corner and lower right corner of Fig. 2c, one could observe similar pore structures observed in Fig. 3a and b. The SAED patterns (insert in Fig. 3c) show only

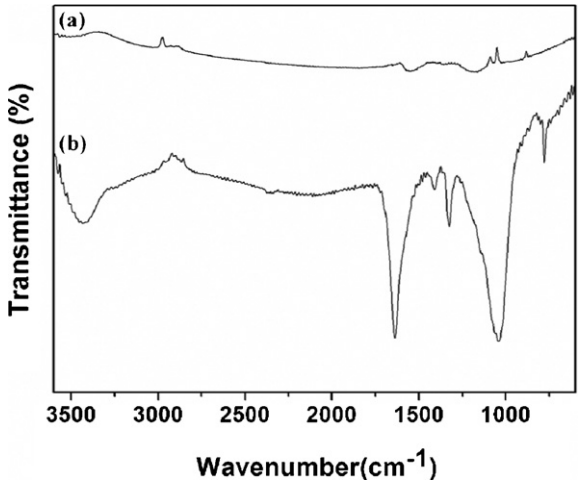

Fig. 2. FTIR spectra of graphene (a) and the 3D-CSGR mesostructures (b).

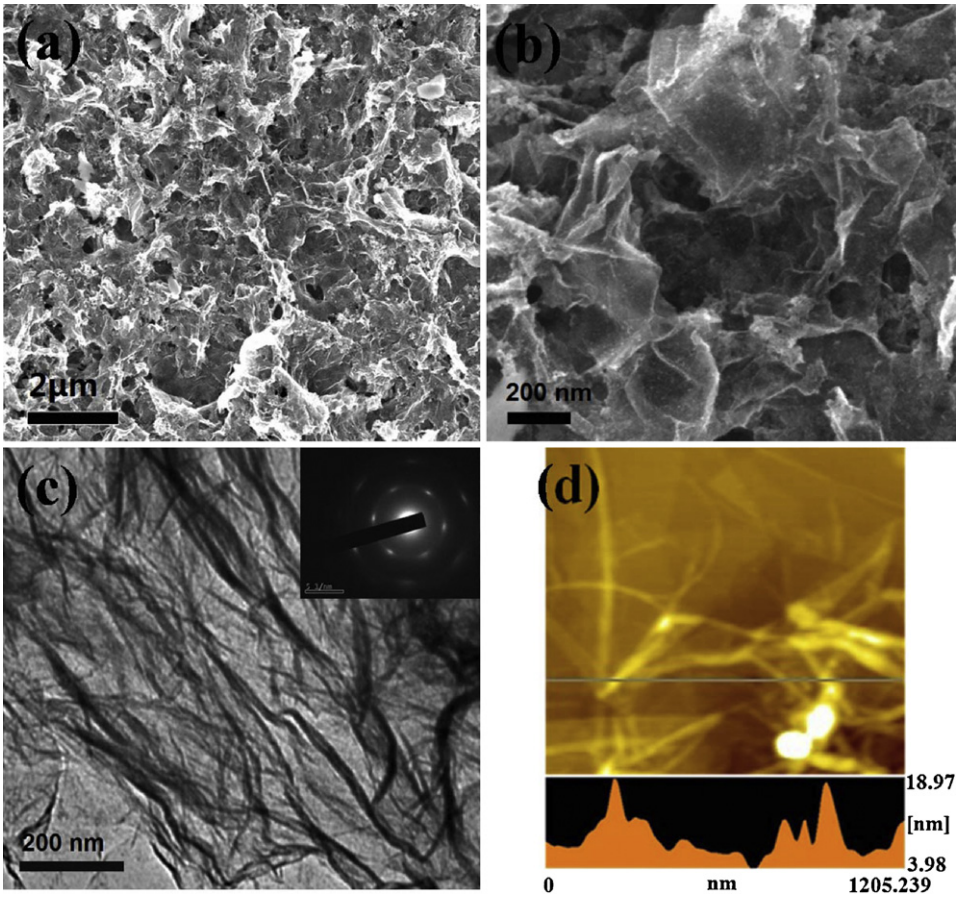

Fig. 3. SEM images (a and b), TEM image (c), the inset shows the SAED pattern of the 3D-CSGR mesostructures, and AFM image (d), of the 3D-CSGR mesostructures.

weak and diffuse rings, indicating the loss of long range ordering in the graphene sheets (Kaniyoor, Baby, & Ramaprabhu, 2010). AFM image in Fig. 3d reveals that the graphene-based composites are highly fluctuant and porous, which is quite different from conventional 2D graphene nanosheet. The depth profile in Fig. 3d shows that the pores sizes vary from 100 nm to 800 nm, which dovetailed nicely with the SEM observations shown in Fig. 3a and b. The depth profile of Fig. 3d also reveals that the depths for these mesoholes are about 15 nm, furthermore indicating the 3D features of the nanocomposites.

Fig. 4a shows the N_2 adsorption–desorption isotherms and BJH pore size distribution plots of the typical 3D-CSGR sample. As we can see in Fig. 4a, the sample has unique mesoporous structures. Fig. 4b indicates that these samples have a broad pore size distribution. Investigations show that the BET surface area of 3D-CSGR is about 603.2 $m^2\ g^{-1}$, which is superior to the low temperature exfoliated graphene (~442.9 $m^2\ g^{-1}$) (Kaniyoor et al., 2010) and CVD derivated graphene (~127.2 $m^2\ g^{-1}$) (Dervishi et al., 2009). Furthermore, the BET surface area of the sample is also obviously higher than the BET surface area of graphene prepared by the widely used Hummers method (202 $m^2\ g^{-1}$) (Fan et al., 2010). This surface area improvement should be mainly due to the successful combination of chitosan with two-fold helix and great amounts of CO_2 and H_2O release in the thermal treatment of the hybrid composites of GO and chitosan.

3.2. Decolorizations of RB5 by 3D-CSGR mesostructures

The photograph in Fig. 5 directly shows the successful decoloration of RB5 by 3D-CSGR. Referring to the deionized water, only very faint black color is recognized in the decolorized solution. The residual RB5 with very low concentration might be regarded as a

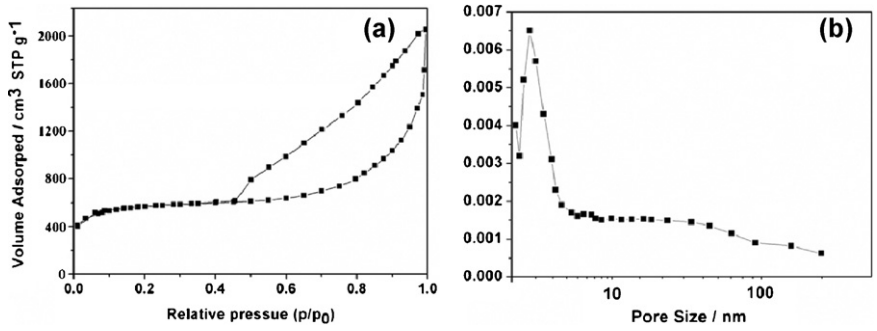

Fig. 4. Nitrogen adsorption/desorption isotherm (a) and pore size distribution (b) of 3D-CSGR mesostructures.

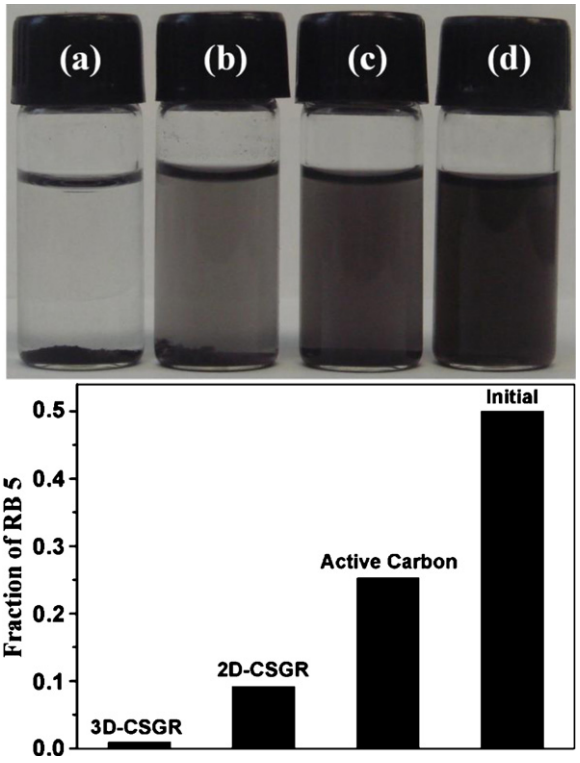

Fig. 5. Dispersion photos for reactive black 5 (0.5 mg/mL): (a) treated and equilibrated with 3D-CSGR mesostructures; (b) treated and equilibrated with CSGR; (c) treated and equilibrated with commercial active carbon and (d) in the absence of any regent. Bottom bar plots show the remaining fraction of RB5 in solution.

priority of absorption over other approaches. Fig. 6 illustrates that the removal efficiencies of RB5 by 3D-CSGR mesostructures were much higher than chitosan functionalized graphene (CSGR) without thermal treatment and commercial active carbon under the same experimental conditions. This may have resulted from some possibilities: Firstly, 3D-CSGR holds higher surface area versus

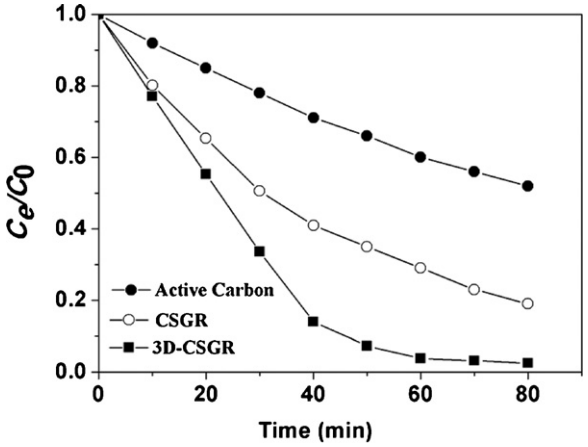

Fig. 6. Removal of RB5 by 3D-CSGR mesostructures. The equilibrium concentration (C_e) was calculated referring to the standard cure of RB5 (the standard curve was drawn based on Lambert–Beer Law: $A = kbc$), C_0 is the initial concentration of RB5. The absorption was fitted to both Langmuir model and Freundlich model. Batch experiments were conducted to compare the efficiencies of 3D-CSGR to decolorize RB5 in aqueous solution. 3D-CSGR (2.0 mL, 0.25 mg/mL, desired pH) was mixed with 4 mL of RB5 (0.2–2 mg/mL) in an erlenmeyer flask. The suspension was incubated at 25 °C for 40 min and standing for another 40 min. The experiment was performed in triplicate and conducted at room temperature. Samples were collected in at 0, 10, 20, 30, 40, 50, 60, 70 and 80 min, respectively: (●) active carbon; (○) CSGR; (■) 3D-CSGR.

CSGR and commercial active carbon, which provided more surface active sites for collision with dye molecules to accelerate the dye removal efficiencies. Secondly, the extended two-fold helix conformation of chitosan in the 3D-CSGR nanocomposites tends to enhanced dye removal efficiency. In the construction processes of 3D-CSGR composites, the chitosan component thermodynamically changes to an extended two-fold helix (the annealed polymorph) conformation together with thermal decomposition of GO and chitosan into CO_2 and H_2O, the spacial two-fold helix conformation of chitosan with aprotic functional groups is helpful for RB5 removal with azo groups. Thirdly, graphene possess excellent electronic properties, which lead to strong electrostatic interactions between 3D-CSGR and the target azo dye RB5, under acidic conditions (pH 6), the analysis of the surface potential of 3D-CSGR (zeta potential −36 mV) confirms the noticeable electrostatic interaction between 3D-CSGR and positive charged RB5. Finally, it was also inferred that by combination with chitosan, there are enhanced hydrogen bonding and van der Waals interactions between 3D-CSGR and RB5, which are also beneficial for RB5 removal. All these possibilities lead to much enhanced removal efficiency of 3D-CSGR for RB5.

Meanwhile, we noticed that for CSGR without thermal treatment, which possesses larger surface area, unique chitosan conformation (hydrated form) and electrostatic force, exhibits better decoloration performance than commercial active carbon, demonstrating the specific advantages of graphene-base materials as adsorbent for azo dyes (Fig. 5).

Removal efficiencies of RB5 by 3D-CSGR at various pHs are shown in Fig. 7a. From the results, we find that pH influences the degradation of RB5 obviously. When pH decreased from 8 to 6 and 4, the removal kinetic rates are increased. Investigations showed that for RB5 removals by 3D-CSGR, reducing pH to 4.0 resulted in the significant elevation of decolorization to more than 2.56% of the original pH (pH 6). Whereas, elevating the pH to 8.0 to dye solution with original pH (pH 6.0) resulted in obvious lower decolorization efficiencies. As a consequence, pH would strongly affect the degradations of RB5 by 3D-CSGR. Such results conform well to literature observations (Chang, Shu, Yu, & Sung, 2006).

The color removals of reactive black 5 by 3D-CSGR mesostructures over 80 min were monitored. Extensive decolorization by 3D-CSGR mesostructures were observed at all the initial dye concentrations ranges from 0.2 mg/mL to 2.0 mg/mL (Fig. 7b). As shown in Fig. 7b, the decolorization process could be divided into two stages: a rapid degradation stage within the first 40 min and a slow decolorization stage thereafter. The dye was removed mainly by absorption during the first stage and the solution became colorless gradually even under high dye concentrations. The second stage contributed about 1.2–18.0% of the color removal. These results imply that at a higher dye concentration (>0.5 mg/mL), with constant 3D-CSGR concentration in the solution, the majority of dye was consumed rapidly in the first 40 min because a higher dye concentration leads to higher probability of adsorption dye molecules. After 40 min, the amount of dye decreases obviously and the degradation efficiency of RB5 slowed down significantly. The fast absorption is another attractive merit of 3D-CSGR over other carbon based RB5 absorbents. For example, the absorption of RB5 with commercial active carbon requires more than 1 h reaching the balance (Qada, Allen, & Walker, 2006).

Fig. 7b also reveals that a increase of initial concentration of RB5 would accelerate the dye decolorization. For example, when the initial concentration of RB5 was changed from 0.5 mg/mL to 1.0 mg/mL, obvious enhanced decoloration efficiency can be observed. However, further increase in initial concentration of RB5 (e.g. from 1.0 mg/mL to 2.0 mg/mL) did not cause any

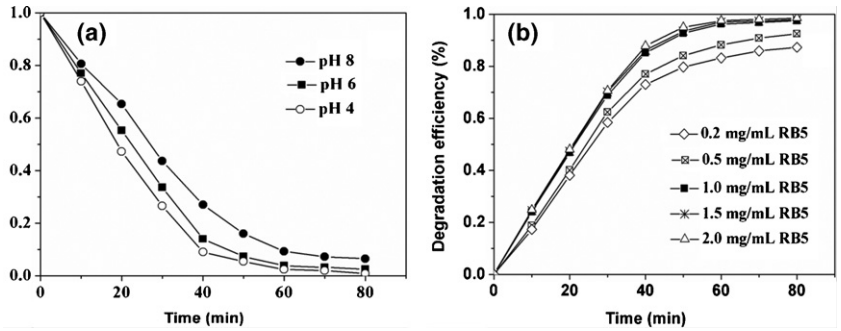

Fig. 7. (a) The effect of pH on removals of RB5 by 3D-CSGR mesostructures: 3D-CSGR (2.0 mL, 0.25 mg/mL, desired pH) was mixed with 4 mL of RB5 (0.2–2 mg/mL) in an erlenmeyer flask. The suspension was incubated at 25 °C for 40 min and standing for another 40 min, (b): Decolorization of reactive black 5 by 3D-CSGR mesostructures at various initial dye concentrations: (◊) 0.2 mg/mL; (⊠) 0.5 mg/mL; (■) 1.0 mg/mL; (*) 1.5 mg/mL and (△) 2.0 mg/mL.

significant change in decolorization efficiency, this could be due to the fact that at higher dye concentration, the dye molecules absorbed rapidly onto the 3D-CSGR composites with mesostructures and large surface area. While the adsorption capacity for the 3D-CSGR mesostructures was constant, the volume of the decoloration solution was also constant, therefore, when lower initial dye concentration was concerned, fewer dye molecules were found in the system with a constant volume, leading to slower molecules movement and much reduced adsorption rate. Because it could decolorize RB5 in wide concentration range with high efficiency, 3D-CSGR mesostructures might be hopefully applied in treating not only the industrial effluent but also the contaminated natural water.

Investigations show that when initial RB5 concentrations are lower than 1 mg/mL, the removal efficiencies are higher than 97.5% and the remnant MB concentration are lower than 0.025 mg/mL. The photograph in Fig. 5 directly shows the successful decoloration of RB5 by 3D-CSGR.

We performed the absorption experiments under different temperatures to evaluate the influence of temperature. The absorption process is more favorable at lower temperatures. At RB5 concentration of 1.0 mg/L, the absorption efficiency is 98.0% mg/g at 0 °C and 97.5% at 25 °C, when the temperature increases to 50 °C, the absorption efficiency of 3D-CSGR further drops to 97.3% mg/g. This phenomenon implies that the absorption is an exothermal reaction. To understand the kinetics and thermodynamics of the absorption process, more efforts are required in future.

4. Conclusion

In conclusion, we have developed a novel and simple thermal method to prepare 3D chitosan–graphene nanocomposites with large specific surface area and unique mesoporosity. By starting from waste sugarcane bagasse derived graphite and chitosan, the resulted composites possess competitiveness in renewable resource recycling and environmental applications. The mesocomposites exhibit high dye-adsorption capacity, which were used to RB5 from aqueous solution. Besides high surface area and unique mesoporous characteristics, the special extended two-fold helix conformation of chitosan component in the 3D-CSGR nanocomposites, the noticeable electrostatic interaction, hydrogen bonding and *van der Waals* interactions between the 3D-CSGR and RB5 would also lead to enhanced removal efficiency of 3D-CSGR for RB5. At initial RB5 concentrations of 1 mg/L, the removal efficiency can achieved to 97.5% and the solution can be decolorized to nearly colorless. Experiments show that the absorption efficiency of 3D-CSGR mesostructures can be regulated by many influencing factors, such as temperature, pH value and the initial concentration of the dye. These results indicate that the 3D-CSGR mesostructures could be applied in treating the industrial effluent and the contaminated natural water.

Acknowledgement

This work was financially supported by the Guangxi Zhuang Autonomous Region Science Foundation of China (No. 200908193).

References

Ahmad, A. L., & Puasa, S. W. (2007). Reactive dyes decolourization from an aqueous solution by combined coagulation/micellar-enhanced ultrafiltration process. *Chemical Engineering Journal*, *132*, 257–265.

Allen, M. J., Tung, V. C., & Kaner, R. B. (2008). Honeycomb carbon: A review of graphene. *Chemical Reviews*, *110*, 132–145.

Barron-Zambrano, J., Szygula, A., Ruiz, M., Sastre, A. M., & Guibal, E. (2010). Biosorption of reactive black 5 from aqueous solutions by chitosan: Column studies. *Journal of Environmental Management*, *91*, 2669–2675.

Bunch, J. S., Zande, A. M., Verbridge, S. S., Frank, I. M., Tanenbaum, D. M., Parpia, J. M., et al. (2007). Electromechanical resonators from graphene sheets. *Science*, *315*, 490–493.

Chandra, V., Park, J., Chun, Y., Lee, J. W., Hwang, I. C., & Kim, K. S. (2010). Water-dispersible magnetite-reduced graphene oxide composites for arsenic removal. *ACS Nano*, *4*, 3979–3986.

Chang, M. C., Shu, H. Y., Yu, H. H., & Sung, Y. C. (2006). Reductive decolorization and total organic carbon reduction of the diazo dye C. I. Acid black 24 by zerovalent iron powder. *Journal of Chemical Technology & Biotechnology*, *81*, 1259–1266.

Chen, Z. P., Ren, W. C., Gao, L. B., Liu, B. L., Pei, S. F., & Cheng, H. M. (2011). Three-dimensional flexible and conductive interconnected graphene networks grown by chemical vapour deposition. *Nature Materials*, *10*, 424–428.

Cheng, J. S., Du, J., & Xu, J. Y. (2011). New role of graphene oxide in the recyclable palladium nanoparticles catalyzed reductive ullmann reaction in environmental friendly ionic liquid/supercritical carbon dioxide system. *Journal of Materials Chemistry*, *21*, 3485–3494.

Cheng, J. S., Tang, T. H., & Li, J. H. (2011). Palladium nanoparticles-decorated graphene nanosheets as highly regioselective catalyst for cyclotrimerization reaction. *Journal of Nanoscience and Nanotechnology*, *11*, 5159–5168.

Crini, G. (2006). Non-conventional low-cost adsorbents for dye removal: A review. *Bioresource Technology*, *97*, 1061–1085.

Dervishi, E., Li, Z. R., Watanabe, F., Biswas, A., Xu, Y., Biris, A. R., et al. (2009). Large-scale graphene production by RF-cCVD method. *Chemical Communications*, 4061–4063.

Du, X. S., Yu, Z. Z., Dasari, A., Ma, J., Mo, M. S., Meng, Y. Z., et al. (2008). New method to prepare graphite nanocomposites. *Chemistry of Materials*, *20*, 2066–2068.

Fan, Z. J., Yan, J., Zhi, L. J., Zhang, Q., Wei, T., Feng, J., et al. (2010). A Three-dimensional carbon nanotube/graphene sandwich and its application as electrode in supercapacitors. *Advanced Materials*, *22*, 3723–3728.

Forgacs, E., Cserháti, T., & Oros, G. (2004). Removal of synthetic dyes from wastewaters: A review. *Environment International*, *30*, 953–971.

Geim, A. K. (2009). Graphene: Status and prospects. *Science*, *324*, 1530–1534.

Ghoreishi, M., & Haghighi, R. (2003). Chemical catalytic reaction and biological oxidation for treatment of non-biodegradable textile effluent. *Chemical Engineering Journal*, *95*, 163–169.

Girgis, B. S., Khalil, L. B., & Tawfik, T. A. M. (1994). Activated carbon from sugar cane bagasse by carbonization in the presence of inorganic acids. *Journal of Chemical Technology and Biotechnology*, *61*, 87–92.

Guo, C. X., Hu, F. P., Lou, X. W., & Li, C. M. (2010). High-performance biofuel cell made with hydrophilic ordered mesoporous carbon as electrode material. *Journal of Power Sources*, *195*, 4090–4097.

Guo, C. X., Lu, Z. S., Lei, Y., & Li, C. M. (2010). Ionic liquid-graphene composite for ultratrace explosive trinitrotoluene detection. *Electrochemistry Communications*, *12*, 1237–1240.

Kaniyoor, A., Baby, T. T., & Ramaprabhu, S. (2010). Graphene synthesis *via* hydrogen induced low temperature exfoliation of graphite oxide. *Journal of Materials Chemistry*, *20*, 8467–8469.

Kawahara, M., Yui, T., Oka, K., Zugenmaier, P., Suzuki, S., Kitamura, S., et al. (2003). Fourth 3D structure of the chitosan molecule: Conformation of chitosan in its salts with medical organic acids having a phenyl group. *Bioscience Biotechnology & Biochemistry*, *67*, 1545–1550.

Lee, S. H., Kim, H. W., Hwang, J. O., Lee, W. J., Kwon, J., Bielawski, C. W., et al. (2010). Three-dimensional self-assembly of graphene oxide platelets into mechanically flexible macroporous carbon films. *Angewandte Chemie International Edition*, *49*, 10084–10088.

Li, X., Wang, X., Zhang, L., Lee, S., & Dai, H. (2008). Chemically derived, ultrasmooth graphene nanoribbon semiconductors. *Science*, *319*, 1229–1232.

Liang, C. D., Li, Z. J., & Dai, S. (2008). Mesoporous carbon materials: Synthesis and modification. *Angewandte Chemie International Edition*, *47*, 3696–3717.

Macquarrie, D. J., & Hardy, J. J. E. (2005). Applications of functionalised chitosans in catalysis. *Industrial & Engineering Chemistry Research*, *44*, 8499–8520.

Masel, R. I. (1996). *Principles of adsorption and reaction on solid surfaces*. Wiley Interscience.

Novoselov, K. S., Jiang, D., Schedin, F., Booth, T. J., Khotkevich, V. V., Morozov, S. V., et al. (2005). Two-dimensional atomic crystals. *Proceedings of the National Academy of Sciences*, *102*, 10451–10453.

Qada, E. N., Allen, S. J., & Walker, G. M. (2006). Adsorption of basic dyes onto activated carbon using microcolumns. *Industrial & Engineering Chemistry Research*, *45*, 6044–6049.

Reina, A., Jia, X. T., Ho, J., Nezich, D., Son, H. B., Bulovic, V., et al. (2008). Large area, few-layer graphene films on arbitrary substrates by chemical vapor deposition. *Nano Letters*, *9*, 30–35.

Ruiz, M., & Rolz, C. (1971). Activated carbons from sugar cane bagasse. *Industrial & Engineering Chemistry Research*, *10*, 429–432.

Stoller, M. D., Park, S., Zhu, Y., An, J. H., & Ruoff, R. S. (2008). Graphene-based ultracapacitors. *Nano Letters*, *8*, 3498–3502.

Stolz, A. (2001). Basic and applied aspects in the microbial degradation of azo dyes. *Applied Microbiology and Biotechnology*, *56*, 69–80.

Sun, W., Guo, C. X., Zhu, Z. H., & Li, C. M. (2009). Ionic liquid/mesoporous carbon/protein composite microelectrode and its biosensing application. *Electrochemistry Communications*, *11*, 2105–2108.

Wang, X., Zhi, L. J., & Müllen, K. (2008). Transparent, conductive graphene electrodes for dye-sensitized solar cells. *Nano Letters*, *8*, 323–327.

Wu, J. H., Pisula, W., & Müllen, K. (2008). Graphenes as potential material for electronics. *Chemical Reviews*, *107*, 718–747.

Xu, Y. X., Bai, H., Lu, G. W., Li, C., & Shi, G. Q. (2008). Flexible graphene films via the filtration of water-soluble noncovalent functionalized graphene sheets. *Journal of the American Chemical Society*, *130*, 5856–5857.

Xu, Y. X., Sheng, K. X., Li, C., & Shi, G. Q. (2010). Self-assembled graphene hydrogel via a one-step hydrothermal process. *ACS Nano*, *4*, 4324–4330.

Xu, Y. X., Wu, Q., Sun, Y. Q., Bai, H., & Shi, G. Q. (2010). Three-dimensional self-assembly of graphene oxide and DNA into multifunctional hydrogels. *ACS Nano*, *4*, 7358–7362.

Yang, S.-T., Chang, Y., Wang, H., Liu, G., Chen, S., Wang, Y., et al. (2010). Folding/aggregation of graphene oxide and its application in Cu^{2+} removal. *Journal of Colloid and Interface Science*, *351*, 122–127.

Zhang, H., Lv, X. J., Li, Y. M., Wang, Y., & Li, J. H. (2010). P25-graphene composite as a high performance photocatalyst. *ACS Nano*, *4*, 380–386.